

**SUPERCritical TESTS OF A SELF-OPTIMIZING,
VARIABLE-CAMBER WIND TUNNEL MODEL***

Ely S. Levinsky
General Dynamics Convair Division

Richard L. Palko
Sverdrup/ARO, Inc.

SUMMARY

A testing procedure has been used in the 16-foot Transonic Propulsion Wind Tunnel (PWT-16T) at the Arnold Engineering Development Center (AEDC) which leads to optimum wing airfoil sections without stopping the tunnel for model changes. Being experimental, the optimum shapes obtained incorporate various three-dimensional and nonlinear viscous and transonic effects presently not included in analytical optimization methods. The present method is a closed-loop, computer-controlled, interactive procedure and employs a Self-Optimizing Flexible Technology (SOFT) wing semispan model that conformally adapts the airfoil section at two spanwise control stations to maximize or minimize various prescribed merit functions (e.g., minimum drag) subject to both equality and inequality constraints (e.g., fixed lift, maximum spanwise differential deflection). The model, which employed twelve independent hydraulic actuator systems (nine functioned) and flexible skins, was also used for conventional testing (Ref. 1). Although six of seven optimizations attempted were at least partially convergent (several of which are shown herein), further improvements in model skin smoothness and hydraulic reliability are required to make the technique fully operational.

INTRODUCTION

Although considerable interest has been generated at this Advanced Technology Airfoil Research conference and in the past in the analytical design of optimum airfoils (e.g., Ref. 2-4), such methods are somewhat approximate, because of the inability of current-generation computers to evaluate the flow field with sufficient accuracy and rapidity. This is especially true under conditions of high lift or supercritical transonic flow, where boundary layer transition, separation and possible reattachment, and shock wave interaction are among the highly nonlinear flow phenomena still beyond analytical solution. In addition, the large number of flow field solutions required for each optimization may preclude analytical optimization of three-dimensional wings, even with the most advanced digital computers.

The present SOFT wing optimization procedure differs from the analytical methods in that the wind tunnel is used as an analog computer, in conjunction with a flexible and controllable

* This work was supported by the U.S. Navy, Office of Naval Research, under Contract N00014-76-C-0742; by the U.S. Air Force Flight Dynamics Laboratory and Arnold Engineering Development Center; and by ARO, Inc.

model, to rapidly generate aerodynamic data, instead of using a digital computer for this purpose. In both cases, the data are then supplied to a computer, which controls and optimizes wing shape by application of nonlinear programming techniques. The SOFT wing procedure will, however, be limited by the extent of wing articulation and degree of shape control that may be obtained with a wind tunnel model.

Under a previous contract for the U.S. Navy (ONR), General Dynamics Convair Division fabricated and tested a two-dimensional flexible airfoil model that could be optimized in the tunnel in a manner similar to that used for the present SOFT wing model. The 2-D model was tested under both low-speed and transonic conditions (Ref. 5), and employed five pairs of hydraulic actuators to vary leading edge radius and camber. Airfoil shape and angle of attack were controlled "on line" to minimize drag, subject to constraints, using the gradient projection optimization algorithm. Satisfactory convergence was found, even with flow separation; however, because of the intermittent blow-down type operation of the transonic test facility, a sequence of individual runs was required to complete a single optimization problem.

The present 3-D SOFT wing model was tested in PWT-16T at AEDC during the summer of 1977. Test Mach numbers ranged from 0.6 to 0.925. The SOFT wing model employed twelve independent hydraulic actuator systems similar in design to those in the 2-D model. The computer-controlled testing and optimization techniques were also similar, but the number of control channels was increased to handle the larger number of independent control variables. Because of the continuous operation of Tunnel 16T, continuous computer control of the wing could be maintained during an optimization, and under ideal circumstances, a single run in the wind tunnel was sufficient to arrive at an optimum wing shape for a prescribed test condition.

The present paper briefly describes the SOFT wing model, closed-loop testing technique and optimization procedure, summarizes several of the optimization problems attempted, and reviews the causes of various difficulties.

SYMBOLS

A_{ij}	Actuator positions in counts ($0 \leq A_{ij} \leq 1000$)
C_D	Drag coefficient
C_L	Lift coefficient
F	Objective function being minimized
g	Vector of constraints
K_i	Stepsize of i^{th} simultaneous mode point
M	Mach number
N	Iteration number
R	Restoration function
S, S_R	Vector search directions
α	Angle of attack
Λ	Lagrange multiplier vector
ϕ	Merit function to be minimized
θ	Independent variables (transformed)
∇	Gradient vector

Superscript

- T Transposed matrix
* Best K; also uncorrected for weight tares

WIND TUNNEL MODEL

The $1/6$ -scale semispan model consisted of an existing fuselage with a flow-through nacelle, an existing horizontal tail surface, and the three-dimensional SOFT wing panel tested at leading edge sweep angle 26° . The wing actuators, shown schematically in Figure 1, are designed to perform the following variations:

- A_{11} Nose radius, inboard station
 A_{12} Nose deflection about 15% chord line, inboard station
 A_{13} Nose deflection about 25% chord line, inboard station
 A_{14} Upper surface humping, inboard station
 A_{15} Trailing edge deflection about 65% chord line, inboard station
 A_{16} Trailing edge deflection about 80% chord line, inboard station
 A_{21} - A_{26} Same as A_{11} - A_{16} , except at outboard stations

All systems except for the A_{14} , A_{21} , and A_{24} actuators remained functional throughout the test, giving a total of ten degrees of freedom, including α . The wing was fabricated with flexible leading edge and trailing edge skins with sliding joints to permit deflections up to 15° (nose) and 30° (trailing edge). The spars, skin sections, and linkages were designed to conform to a specific target shape designated T-1 with the actuators set at the nominal positions (Figure 2). Other target shapes designated (T), envelope (E), parametric (P) and optimum (O) wing shapes tested are listed in Table 1.

The model was mounted horizontally and inverted off a sharp edge reflection plane supported from the wind tunnel sidewall. The model is shown fully assembled and installed as tested in Figure 3.

CLOSED-LOOP TEST PROCEDURE

A closed-loop testing technique was employed to set wing shape from the time that the skins were installed to avoid damaging the model. The block diagram of Figure 4 shows the basic elements of the control system and computer linkup. All actuator position changes were made through the PWT DEC System 10 computer, both for conventional and optimization runs. Conventional runs were made either by stepping the actuators through a prescribed sequence of positions at fixed α and M , or by holding the actuators fixed and stepping α through a prescribed schedule.

In general, the tunnel was run continuously while making airfoil shape changes between runs and while changing from conventional to optimization runs. Thus, even for conventional tests, the SOFT wing showed promise of being highly efficient and productive in that no tunnel down time was required to make model changes.

For optimization testing, the optimization program played a central role in that it generated the commands for changing the A_{ij} and α settings, as described below.

OPTIMIZATION PROGRAM

A flow chart of the optimization procedure, which was based on the gradient projection optimization algorithm, is presented in Figure 5. The optimization program operates in two distinct modes: "incremental" and "simultaneous." Only the incremental mode is used during the initial iteration (and restarts), during which each active actuator and angle of attack is perturbed individually to generate gradient vectors $\nabla\phi$ and ∇g of the merit function and active constraints, respectively. The number of incremental mode points per iteration depends on the number of active actuators and on the number of times the perturbations are repeated to improve accuracy (termed "cycling"). With 9 active actuators, there were 11 incremental mode points per cycle.

After the incremental mode, the vector directions S_R or S , for either restoring the constraints $g = 0$ or minimizing the objective function F during the next iteration, depending upon whether any constraints were violated at the nominal incremental mode point, are calculated by the gradient projection algorithm, which gives in matrix form:

$$F = -\phi + g \Lambda$$

$$S = -\nabla F$$

$$S_R = \nabla g (\nabla g^T \nabla g)^{-1} g$$

and

$$\Lambda = -(\nabla g^T \nabla g)^{-1} \nabla g^T \nabla \phi$$

The next iteration begins with the simultaneous mode, during which all active actuators and α are advanced together in the direction S or S_R , as obtained from the previous iteration, through a sequence of up to 11 test points of step size K_i . The sequence is aborted if any of the constraints are violated by more than the prescribed tolerance. Upon completion of the stepping, the computer selects the "best" of the simultaneous mode points K^* (either minimum $R = gg^T$ or minimum F), and then resets the wing shape to that configuration. The incremental mode is then repeated in preparation for the next iteration.

CONVENTIONAL RUNS

Only the conventional run data comparing the SOFT wing T-1 shape with a comparable solid-wing model equivalent to the W_{52} theoretical shape shown in Figure 2 will be presented. Figure 6 shows that wing shape T-1 experienced significantly higher drags, particularly at the higher Mach numbers, even though T-1 was set to match the W_{52} theoretical shape as closely as possible. The higher drag was most likely caused by the leading edge sliding skin joint (lap) of approximately 0.13 cm thickness that protruded out of contour on the upper surface, by a bulge that protruded out of contour in the outboard region of the aft lower surface, and by deviations in nose shape. The deviations in Figure 2 between the pre- and post-test T-1 shapes may account for the scatter band in Figure 6, since the flow at transonic conditions is highly sensitive to small changes in airfoil shape (Ref. 2). It is planned to improve the SOFT wing model for subsequent tests to approach solid model drag levels.

OPTIMIZATION RUNS

The optimization problems are summarized in Table 2, which lists Mach number, merit function, active constraints, convergence assessment, iteration number N considered optimum, and the percentage reduction in merit function. Each optimization problem was initiated with the

wing set at the T-1 target shape; the percentage of C_D^* decrease is with respect to the T-1 shape tested during the same (or closest) run sequence.

Weight tare corrections were inadvertently omitted during the on-line data reduction used to steer the direction of wing optimization. Consequently, evaluations of convergence were based upon uncorrected coefficients C_L^* and C_D^* , rather than on C_L and C_D . This error biased the optimization procedure in favor of increasing α at the expense of aft camber.

Only optimization Problem 4-2 (completed as Problem 30) will be discussed in detail. It deals with minimizing C_D^* for $C_L^* = 0.50$, subject to various inequality constraints on the actuators at Mach 0.85. As shown in Figure 7, Problem 4-2 was continued for six iterations, after which a premature shutdown was experienced, due to lubrication difficulties with a main compressor bearing. The optimization was then continued as Problem 30, without reinitialization. Figure 7 shows a graphical representation of the convergence process. All constraints are satisfied for the iterations represented by solid symbols, while the open symbols signify that at least one constraint has been violated. Iteration 17 is readily seen to have the lowest value of C_D^* with all constraints satisfied; it was, therefore, selected as optimum. The gap between Iterations 6 and 7 in Figure 7 was caused by the low q while the tunnel was shutting down during Iteration 6. The double values for C_D^* during Iterations 12 and 14 and the poor convergence displayed during this period were the result of excessive shifts in the A_{15} actuator position.

Variations of each functional actuator, α , and various dependent data functions during iteration $N = 11$ from Problem 30 are shown in Figure 8. The iteration, during which C_D^* is minimized, contains 11 simultaneous and 22 incremental mode points cycled twice. The precise control of actuator positions and the good repeatability of the aerodynamic data during the two incremental mode cycles are apparent.

Convergence in the C_L^*, C_D^* plane is shown in Figure 9. Also shown are the drag polars for the T-1 wing shapes run just before and after the optimization run, and that made with the optimum wing O-30 (Iteration 17). The advantage of the O-30 wing shape over T-1 at the design C_L^* is clearly apparent. Unfortunately, this same reduction was not found in C_D because of the tare effects referred to previously. A correction for tare effects (made after the test for iteration $N = 4$) showed that increased trailing edge deflections, decreased angles of attack, and decreased values of C_D would have been obtained with the tare correction included (Figure 10).

Similar optimization results are shown in Figures 11 through 18 for problems 3-2, 41-2, and 4-3 of Table 2. Problem 3-2 is similar to 4-2 and 30, except for reduced articulation (only the A_{12} , A_{15} , A_{22} , and A_{25} actuators were varied, subject to $A_{12} = A_{22}$ and $A_{15} = A_{25}$). Figure 11 demonstrated excellent convergence, although the C_D^* improvement ($N = 20$) was now much less. The reduced articulation is apparent in Figure 12 (iteration $N = 18$), which also shows that the simultaneous mode was aborted after the ninth point of this iteration because the constraint on $A_{15}-A_{25}$ was violated. Figure 13 shows that the C_D^* reduction for the optimum wing shape designated O-3.2 persisted over a wide range of C_L .

Problem 41-2 dealt with minimizing C_D^* at $C_L^* = 0.25$ with full model articulation. Excellent convergence was obtained, and iteration $N = 29$ was selected as optimum (Figure 14). Iteration $N = 21$ (Figure 15) is an example of a restoration. Note that all active constraints C_L^* and $|A_{ij} - A_{2j}|$ are restored within tolerance during the simultaneous mode. The convergence of Problem 41-2 in the C_L^*, C_D^* plane is shown in Figure 16.

Optimization Problem 4-3 was similar to 4-2 and 30, except that $M = 0.90$ instead of 0.85. Convergence in this case was rapid, as shown in Figure 17, with $N = 10$ selected as optimum. The corresponding wing shape O-4.3 shows a considerable improvement over the T-1 wing, as seen in Figure 18.

The resultant optimum wings are compared with T-1 in Figure 19. Although the weight tare biased the optimum shapes toward decreased aft camber, the increased leading edge droop of the optimum shapes, especially outboard, may well signify a shape modification that leads to lower drag at moderate to high C_L . On the other hand, Problems 42 and 10 (Table 2) showed marginal and no convergence, respectively. Both problems were attempted at high C_L and showed evidence of reduced control precision, possibly due to the high airloads on the actuators and/or buffeting. Further testing with an improved SOFT wing model is planned to overcome some of these difficulties and make experimental wing optimization an operational tool for the aircraft designer.

CONCLUSIONS

A first attempt has been made at developing an experimental 3-D wing optimization procedure involving a computer-controlled SOFT wing wind tunnel model. Although six of seven optimization problems attempted were at least partially convergent, difficulties were uncovered with deviations in airfoil contour, inadequate control precision at high C_L , and hydraulic system reliability, which increased drag levels and slowed or prevented convergence. Nevertheless, the SOFT wing technique appears to promise a means of generating optimum airfoil and wing shapes, which include all aerodynamic nonlinearities and viscous effects, with a saving in test time and which might not be found by conventional testing or by numerical optimization. Of course, any optimum wings will be limited by model articulation, and will reflect effects of tunnel wall interference, test Reynolds number and model deformation under airload. Plans call for improving the model and performing further tests to make the technique more operational.

REFERENCES

1. Levinsky, E. S. and Palko, R. L.: "Semispan Wind Tunnel Test of a Computer-Controlled Self-Optimizing Flexible Technology Wing," AIAA Paper 78-786, presented at AIAA Tenth Aerodynamic Testing Conference, April 19-21, 1978.
2. Johnson, R. R. and Hicks, R. M.: "Application of Numerical Optimization to the Design of Advanced Supercritical Airfoils," Advanced Technology Airfoil Research, Volume I, NASA CP-2045, Pt. 1, 1979.
3. Lores, M. E.; Burdges, K. P.; Shrewsbury, G. D.; and Hicks, R. M.: "An Evaluation of Numerical Optimization in Supercritical Airfoil Modification and Design," Advanced Technology Airfoil Research, Volume II, NASA CP-2046, 1979.
4. Hicks, R. M.; Murman, E. M.; and Vanderplaats, G. N.: "An Assessment of Airfoil Design by Numerical Optimization," NASA TMX-3092, July 1974.
5. Levinsky, E. S.; Schappelle, R. H.; and Pountney, S.: "Transonic Testing of a Self-Optimizing Flexible Airfoil," Proceedings of the AIAA Ninth Aerodynamic Testing Conference, June 7-9, 1976.

TABLE 1.- SOFT WING SHAPES TESTED

Designation	Wing Type	A ₁₁	A ₁₂	A ₁₃	A ₁₄	A ₁₅	A ₁₆	A ₂₁	A ₂₂	A ₂₃	A ₂₄	A ₂₅	A ₂₆	
T-1	Target No. 1	250	250	250	X	250	250	X	250	250	X	250	250	VAR
T-2	Target No. 2	250	125	143	X	350	60	X	176	94	X	400	56	VAR
T-3	Target No. 3	250	250	250	X	332	456	X	250	250	X	256	547	VAR
E-1	Min Deflection Envelope	100	100	97	X	98	98	X	100	102	X	99	100	VAR
E-2	Max Deflection Envelope	398	401	403	X	799	801	X	401	402	X	798	796	VAR
E-3	Max Diff. Twist Envelope	250	250	250	X	250	250	X	450	250	X	450	250	VAR
P-1	T-1 + $\delta_{TE} = 2.6^\circ$	250	250	250	X	390	250	X	250	250	X	390	250	VAR
P-2	T-1 + $\delta_{TE} = 5.6^\circ$	250	250	250	X	530	250	X	250	250	X	530	250	VAR
P-3	T-1 + $\delta_{LE} = 4^\circ$	250	450	250	X	250	250	X	450	250	X	250	250	VAR
P-4	T-1 + $\delta_{LE} = 7^\circ$	250	600	250	X	250	250	X	600	250	X	250	250	VAR
O-30	Optimum, Problem 30	332	249	536	X	109	73	X	373	530	X	314	127	6.77
O-3.2	Optimum, Problem 3-2	250	417	250	X	131	250	X	490	250	X	131	250	5.71
O-6.2	Optimum, Problem 6-2	437	307	567	X	30	40	X	408	509	X	182	143	6.88
O-41.2	Optimum, Problem 41-2	733	589	272	X	112	60	X	586	291	X	111	68	4.70
O-41.2A	Optimum, Problem 41-2	783	500	374	X	48	112	X	575	230	X	144	69	4.96
O-42	Optimum, Problem 42	293	546	277	X	266	530	X	579	253	X	255	478	6.96
O-4.4	Optimum, Problem 4-3	417	381	561	X	147	235	X	539	404	X	235	240	7.07

T - Target wing; E - Envelope wing; P - Parametric wing; O - Optimum wing

TABLE 2.- SUMMARY OF OPTIMIZATION
PROBLEMS: AEDC 457

Problem No.	Mach No.	Merit Function	Active Constraints	Convergence Properties	Best N	% C _D Decrease from Standard Wing
30	0.85	Min C _D *	C _L = 0.5, Δ Twist $\leq 4^\circ$	Good	17	16%
3-2	0.85	Min C _D *	C _L = 0.5, "Reduced" Articulation, Δ Twist = 0°	Excellent	20	6%
41-2	0.85	Min C _D *	C _L = 0.25, Δ Twist = 0 \pm 2°	Excellent	29	17%
4-3	0.90	Min C _D *	C _L = 0.50, Δ Twist $\leq 3^\circ$	Excellent	10	14%
42	0.85	Min C _D *	C _L = 0.70, Δ Twist = 0 \pm 2°	Very marginal except for last 4 iterations	33	9%
6-2	0.85	Min C _D *	C _L + C _M /2.3 = 0.50, Δ Twist $\leq 3^\circ$	Excellent up to N = 8 Poor for N > 9	8	18%
10	0.90	Max C _L *	C _D * = 0.11, Δ Twist $\leq 3^\circ$	Poor	None	X

C_D* = C_D - 0.0494 α (deg)

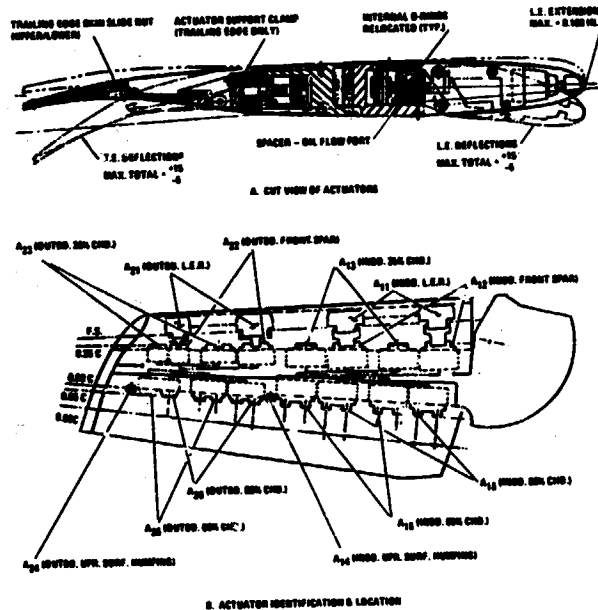


Figure 1.- Three-dimensional wing model hydraulic actuator system.

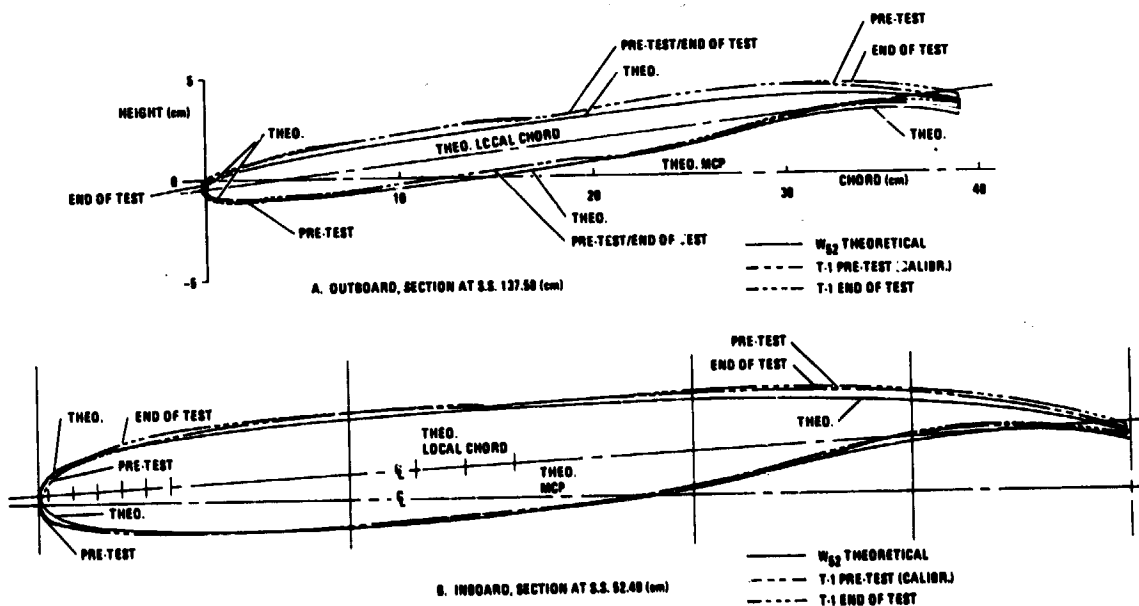


Figure 2.- T-1 actual and theoretical wing shape.

ORIGINAL PAGE IS
OF POOR QUALITY

ORIGINAL PAGE IS
OF POOR QUALITY



Figure 3.- Three-dimensional wing model installed in tunnel.

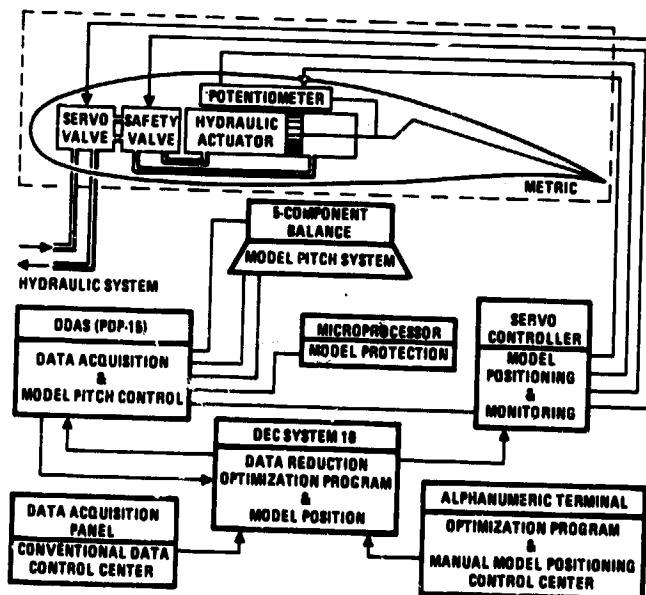


Figure 4.- SOFT wing closed-loop testing procedure.

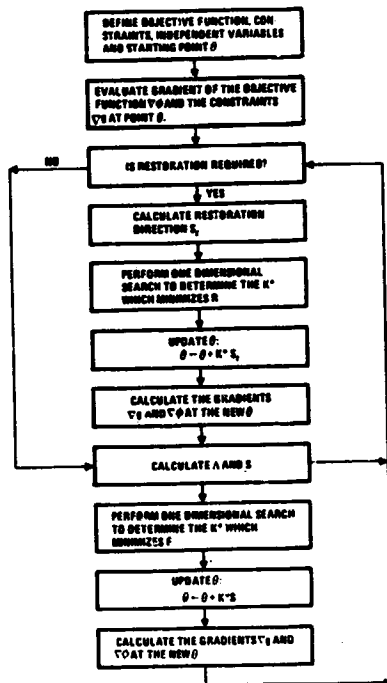


Figure 5.- Flow chart of mathematical optimization procedure.

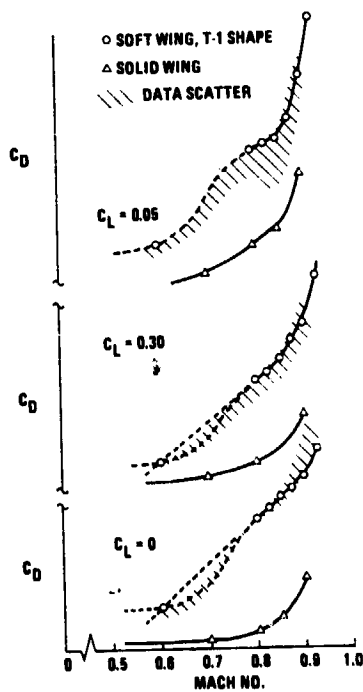


Figure 6.- SOFT wing and solid wing drag variations.

ORIGINAL PAGE IS
OF POOR QUALITY

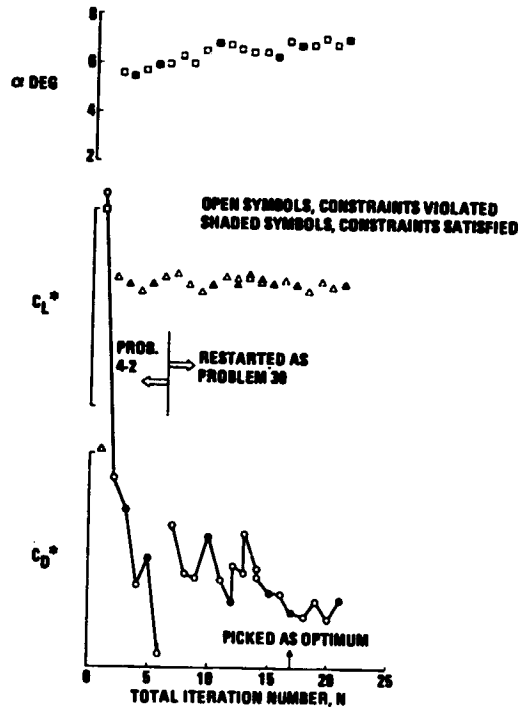


Figure 7.- Optimization summary. Problems 4-2 and 30. Minimum C_D at $C_L = 0.5$; Mach 0.85.

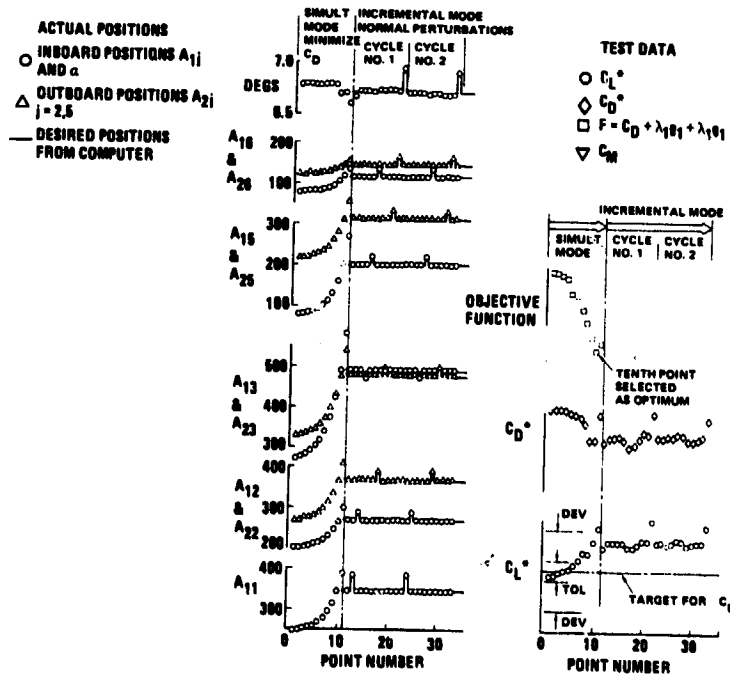


Figure 8.- Minimization of C_D . Iteration N = 11 of problem 30.

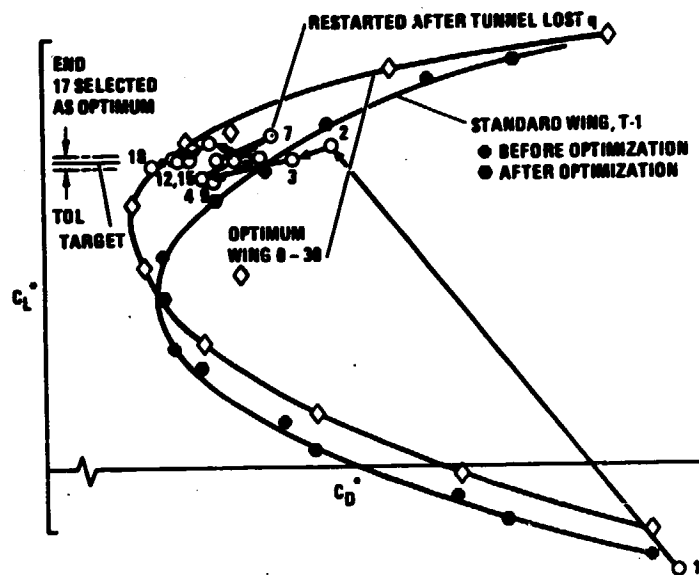


Figure 9.- Problems 4-2 and 30 in C_D^* , C_L^* plane.

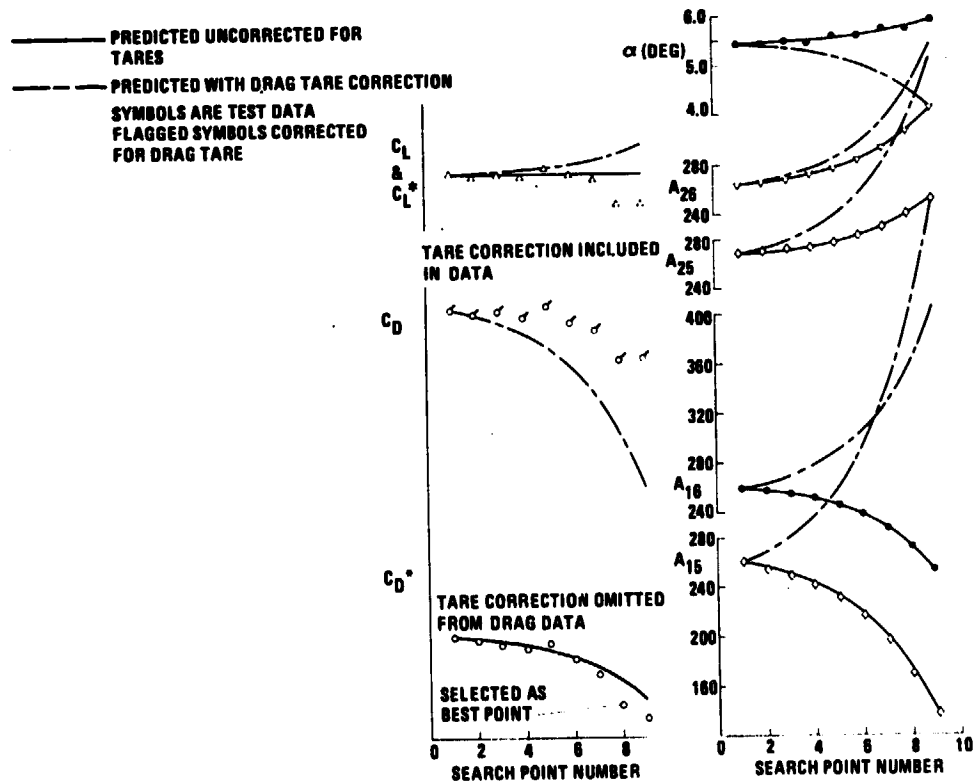


Figure 10.- Tare corrections for iteration 4 of problem 4-2.

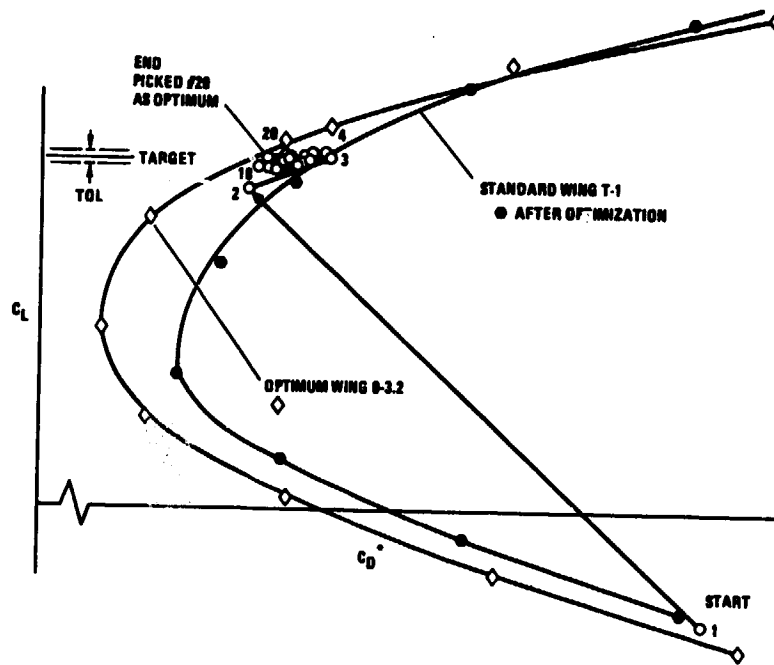


Figure 13.- Problem 3-2 in C_D^* , C_L^* plane.

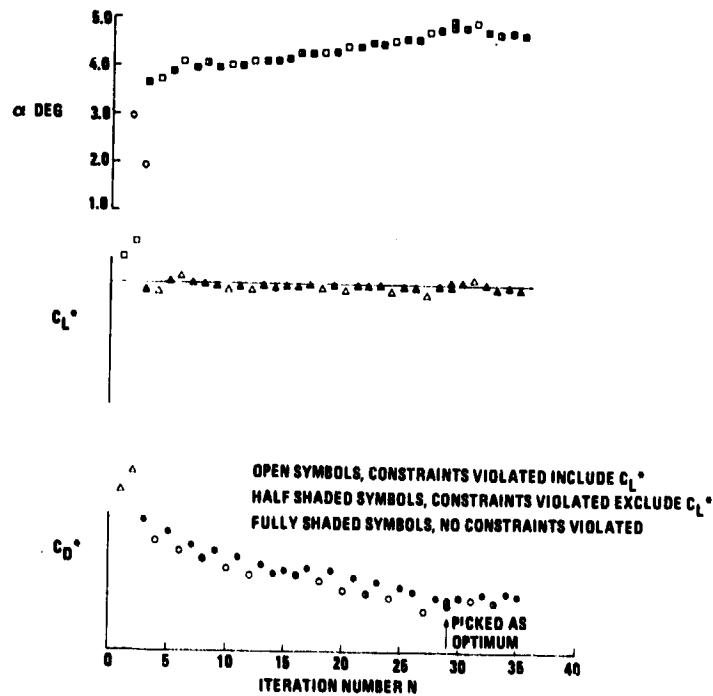


Figure 14.- Optimization summary. Problem 41-2. Minimum C_D at $C_L = 0.25$; Mach 0.85.

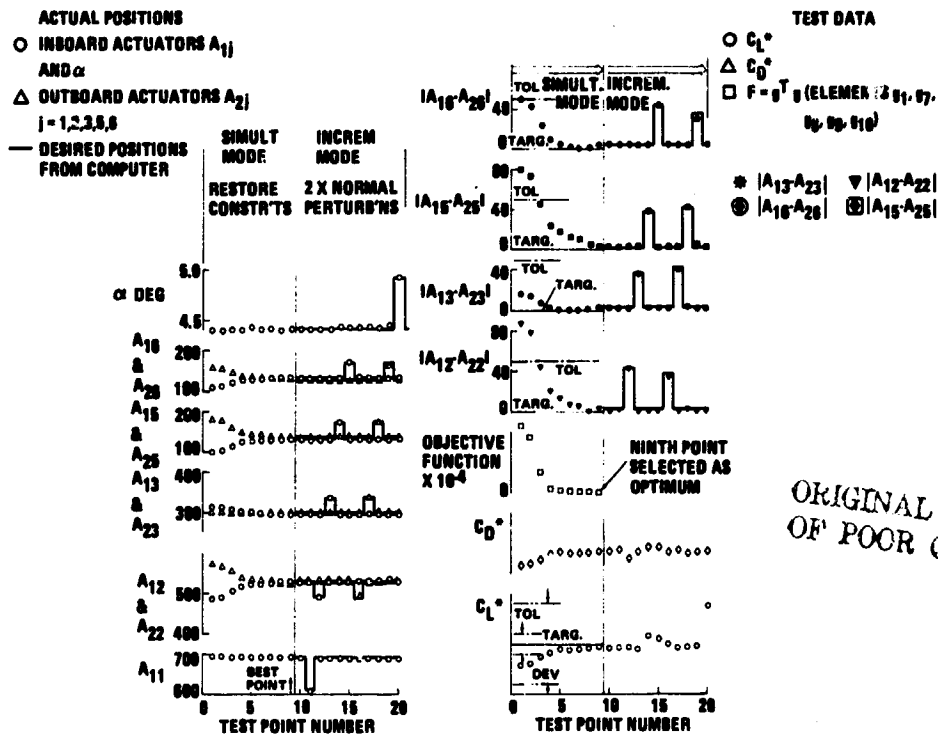


Figure 15.- Restoration of equality constraints on C_L . Iteration $N = 21$ of problem 41-2.

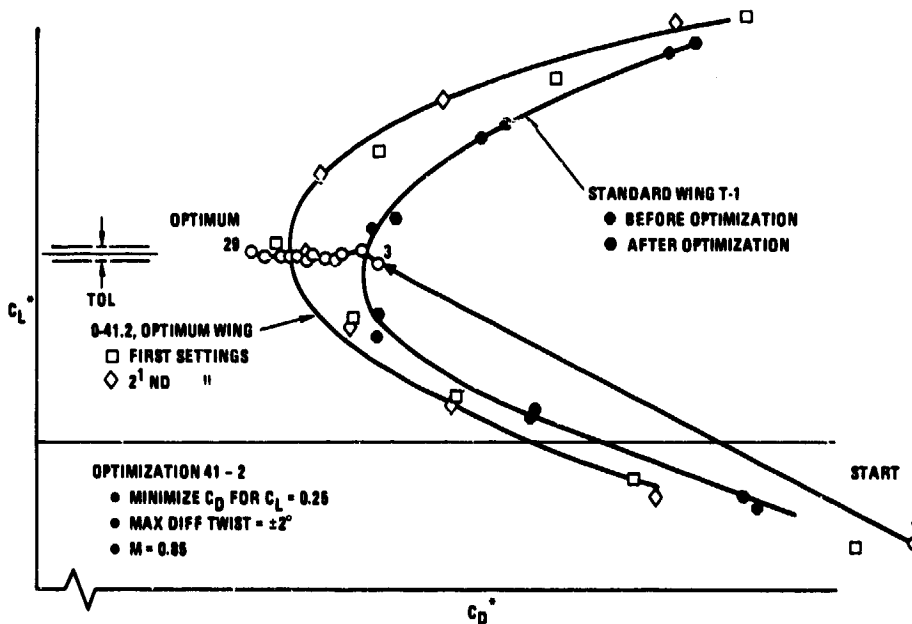


Figure 16.- Problem 41-2 in C_D^* , C_L^* plane.

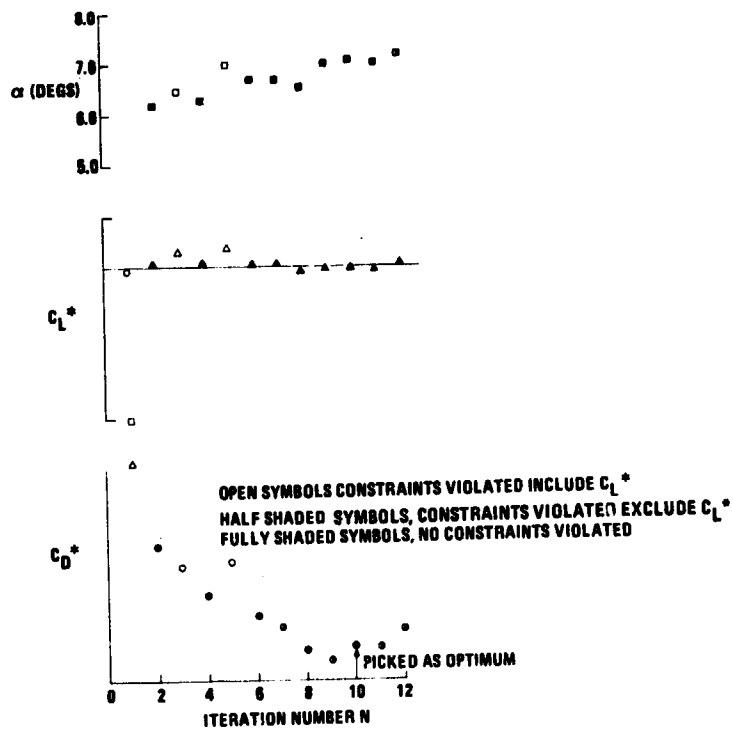


Figure 17.- Optimization summary. Problem 4-3. Minimum C_D at $C_L = 0.5$; Mach 0.9.

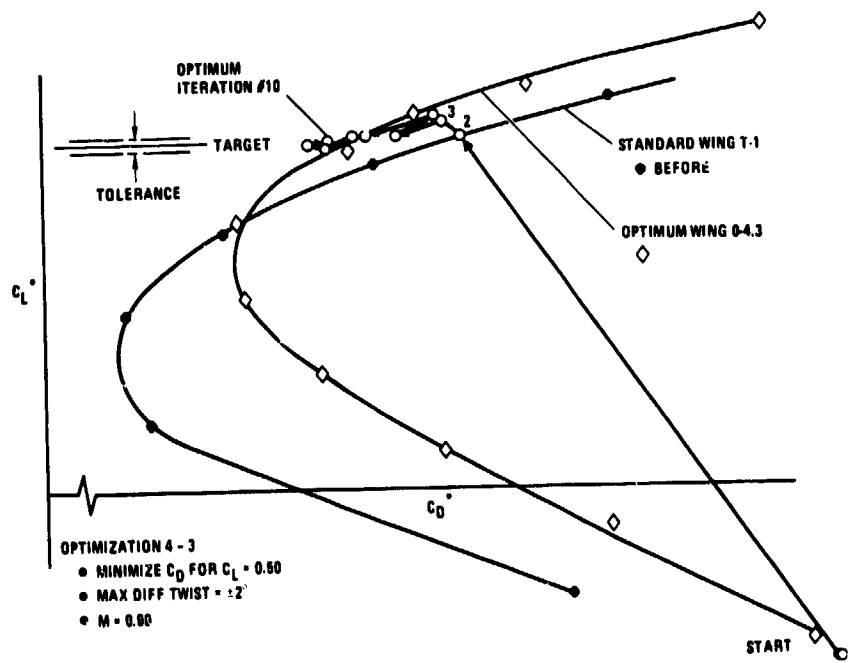


Figure 18.- Problem 4-3 in C_D^* , C_L^* plane.

ORIGINAL PAGE IS
OF POOR QUALITY

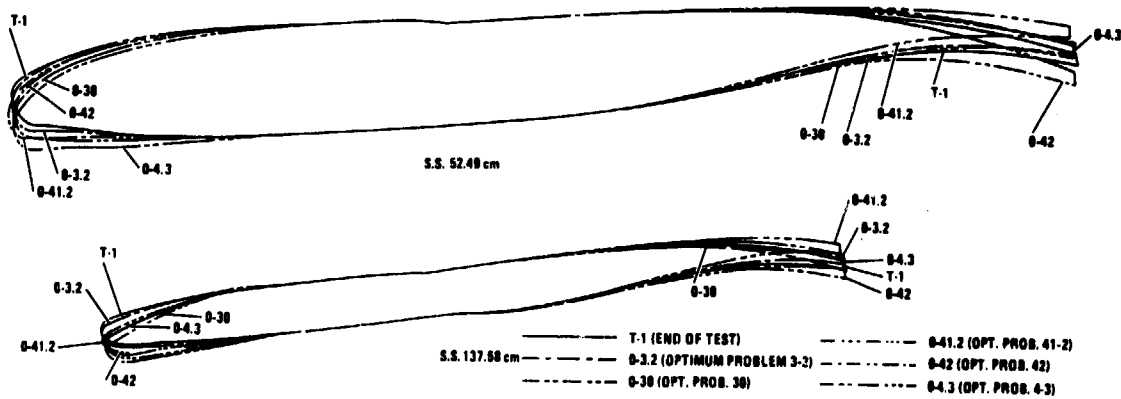


Figure 19.- Optimum wing shapes.